NANO LETTERS

Letter

pubs.acs.org/NanoLett

Versatile Polarization Generation with an Aluminum Plasmonic Metasurface

Pin Chieh Wu,[†,‡] Wei-Yi Tsai,[‡] Wei Ting Chen,[‡] Yao-Wei Huang,[†] Ting-Yu Chen,[‡] Jia-Wern Chen,[‡] Chun Yen Liao,[‡] Cheng Hung Chu,[†] Greg Sun,[§] and Din Ping Tsai*[,†,‡,∥]

[†]Research Center for Applied Sciences, Academia Sinica, Taipei 11529, Taiwan

[‡]Department of Physics, National Taiwan University, Taipei 10617, Taiwan

[§]Department of Engineering, University of Massachusetts Boston, Boston, Massachusetts 02125, United States

[∥]College of Engineering, Chang Gung University, Taoyuan 33302, Taiwan

Supporting Information

ABSTRACT: All forms of light manipulation rely on light−matter interaction, the primary mechanism of which is the modulation of its electromagnetic fields by the localized electromagnetic fields of atoms. One of the important factors that influence the strength of interaction is the polarization of the electromagnetic field. The generation and manipulation of light polarization have been traditionally accomplished with bulky optical components such as waveplates, polarizers, and polarization beam splitters that are optically thick. The miniaturization of these devices is highly desirable for the development of a new class of compact, flat, and broadband optical components that can be integrated together on a single photonics chip. Here we demonstrate, for the first time, a reflective metasurface polarization generator (MPG) capable of producing light beams of any polarizations all from a linearly polarized light source with a single optically thin chip. Six polarization light beams are achieved simultaneously including four linear polarizations along different directions and two circular polarizations, all conveniently separated into different reflection angles. With the Pancharatnam−Berry phase-modulation method, the MPG sample was fabricated with aluminum as the plasmonic metal instead of the conventional gold or silver, which allowed for its broadband operation covering the entire visible spectrum. The versatility and compactness of the MPG capable of transforming any incident wave into light beams of arbitrary polarizations over a broad spectral range are an important step forward in achieving a complete set of flat optics for integrated photonics with far-reaching applications.

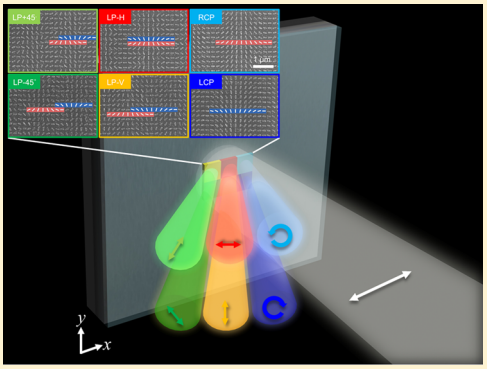

KEYWORDS: *Metasurfaces, aluminum plasmonics, polarization generator, nanoantennas, background-free, Pancharatnam−Berry phase modulation*

Since its discovery in the early 19th century, polarization as one of the key properties of an electromagnetic wave has been used in a wide variety of applications from glare-reducing glasses and liquid-crystal displays[1] to optical signal processing,[2] all of which have had a profound impact in our modern day life. The simplest way of generating a polarized light is to use a polarizer that functions as an optical transmissive filter to allow light of a specific polarization pass but blocking waves of other polarizations. Such a device generates linearly polarized light at the expense of brightness as wave intensity contained in the perpendicular polarization is simply lost.[3] Ideally, one would prefer a polarization generator capable of preserving as much as possible the power intensity contained in the incident waves of all polarizations and converting them into a beam or a set of beams of well-defined polarizations. Such an optical component is obviously desirable when signal strength is a matter of concern for applications involving manipulation of polarizations of weak electromagnetic waves oftentimes found in optical characterization,[4] sensing,[5] quantum computation,[6] 3D imaging,[7] and so forth. Relative to the linear polarization (LP) where the oscillation of its electric field lies along a single line, circular polarization (CP) whose field rotates either clockwise or counter clockwise is intrinsically more difficult to produce because of the required additional phase delay between the two orthogonally linearly polarized wave components. Conventional methods, such as birefringence, all rely on phase retardation that is gradually accumulated as light propagates through an optical medium over a distance much longer than its wavelength. As such, a significant thickness must be provided in order to obtain the needed phase retardation which dictates that nearly all optical components based on these conventional methods of manipulating polarizations are

Received: October 24, 2016
Revised: November 22, 2016
Published: December 5, 2016

DOI: 10.1021/acs.nanolett.6b04446
Nano Lett. 2017, 17, 445−452

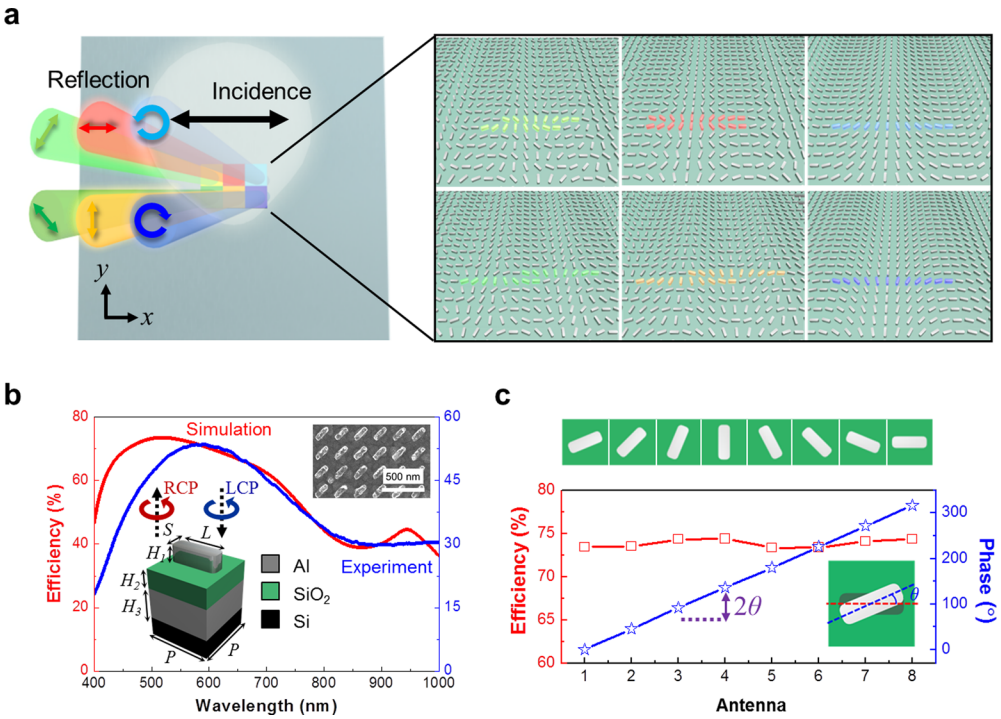

Figure 1. Polarization conversion with aluminum plasmonic metasurfaces. (a) Schematic for arbitrary polarization generation with fixed incident polarization. (b) Simulation and measurement results for the LCP-to-RCP conversion efficiency by an Al nanoantenna array deposited on SiO_2/Al/Si substrate over the spectral range of 400−1000 nm. The simulation is conducted on the nanoantenna array with the unit-cell dimensions of length L = 170 nm, width S = 50 nm, thickness H_1 = 50 nm, and period P = 230 nm that are deposited on SiO_2 layer with thickness H_2 = 50 nm and Al mirror thickness H_3 = 150 nm. The measurement is performed on a sample whose scanning electron microscope (SEM) image is shown in inset. (c) Conversion efficiency and phase modulation for Al nanoantennas of equal dimensions oriented at various angles at wavelength λ = 500 nm. Each data point represents an array of Al nanoantennas all oriented at a fix angle θ.

inevitably bulky. In addition, these bulky devices are always designed to perform only a single functionality; in the case of a polarizer, it yields light output in one particular polarizing state. Needless to say, a versatile, compact polarization generator capable of producing multiple polarizing states is highly desirable.

Metamaterials have been extensively explored in recent years due to their exotic electromagnetic properties, such as negative refraction,[8] cloaking,[9] Fano resonance,[10] toroidal dipolar response,[11] and so on. A number of studies have demonstrated CP light using complex three-dimensional (3D) chiral metamaterials such as multilayer gold spirals.[12,13] While these designs are capable of polarization modulation, there are a number of disadvantages: (1) structures are optically thick as they still rely on light propagation in the media to accumulate phase; (2) light output is significantly attenuated at visible wavelengths because of the need for light to propagate through the plasmonic metamaterials with notoriously associated metal loss; and (3) the fabrication of the 3D structures is extremely complex. These factors fundamentally and technically limit their development and ultimately their scope of applications in optical systems, especially in integrated photonics, as efficient and compact polarizers. In contrast to 3D metamaterials, a metasurface capable of inducing abrupt modulation of the wavefront as it bounces off from it offers a promising alternative for manipulating polarization.[14] The phase modulation required for generating a particular polarization is typically obtained within a subwavelength skin depth of the metasurface in such a reflective scheme, making it possible to achieve flat, ultrathin polarization generators. So far a few flat optical components such as waveplates[15,16] and focusing lens[17,18] have been demonstrated with the use of metasurfaces patterned with noble metals such as gold (Au) and silver (Ag). The working wavelengths of these flat components are largely limited to spectral regimes longer than visible in order to avoid the substantial loss associated with the interband transitions in these metals in the visible range. It has been suggested that aluminum (Al) may be used as the metallic material of choice in a range of plasmonic devices and metasurfaces, expanding their operation into the visible and even UV regimes[19,20] where the photon energies are higher than interband transition energies in Al so that significantly reduced absorption can be achieved in comparison with Au and Ag, leading to the possibility of flat optics, color printing, and hologram made of Al metasurfaces covering the whole spectral range of visible light.[21−23]

In this work we numerically and experimentally demonstrate a metasurface polarization generator (MPG) that transforms a linearly polarized light into six states of polarization in the visible range with the use of Al plasmonics. It should be noted that the functionality of the proposed MPG is obviously not limited to this particular demonstration. In fact, the salient feature of the MPG is its ability to generate multiple light beams of any polarizations from a single source of any specific polarization scattered from a single properly designed MPG device. In this demonstration, the polarizing state of the scattered light is fully controlled with the superposition between CPs (see Figure 1a) of equal amplitude that undergoes 0-to-2π phase modulation by the metasurface. We have employed the Pancharatnam−Berry (P−B) phase[24] (also

DOI: 10.1021/acs.nanolett.6b04446
Nano Lett. 2017, 17, 445−452

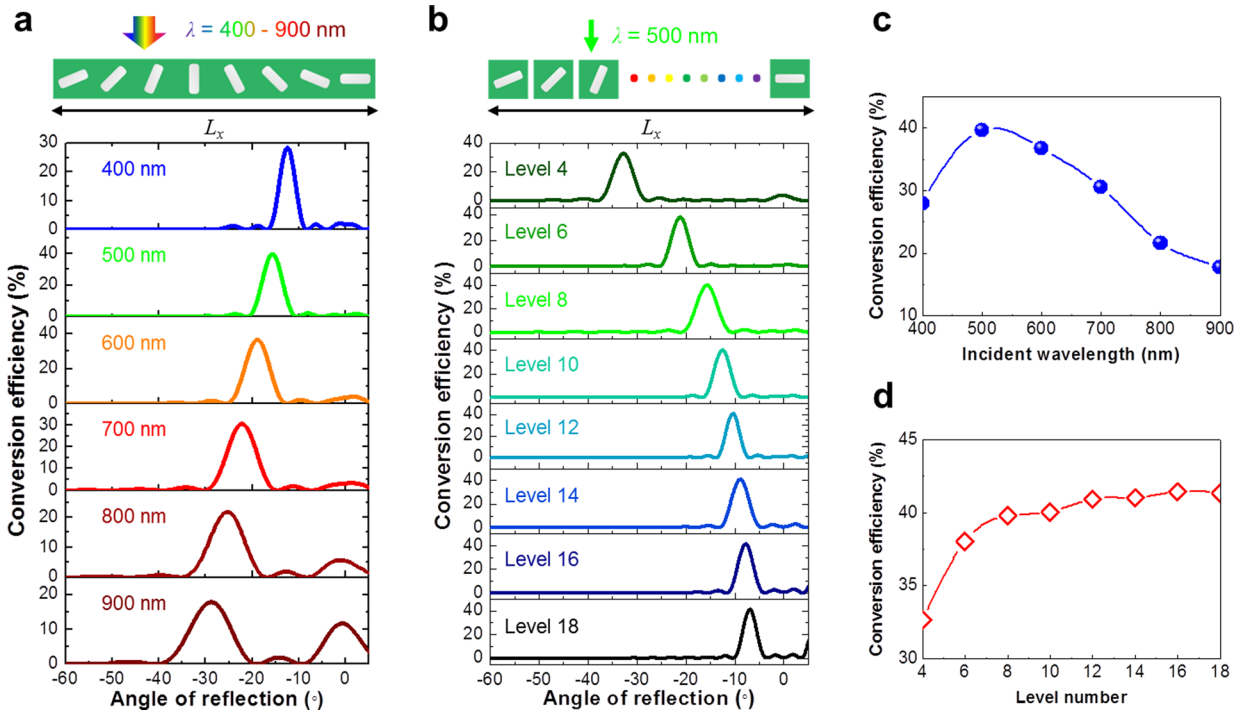

Figure 2. Simulated conversion efficiency and angle of reflection associated with incident wavelength and level number of phase gradient. Conversion efficiency and angle of reflection by (a) a MPG with a fixed supercell length (L_x = 230 nm × 8 = 1840 nm) for a range of incident wavelengths; (b) a MPG of different lengths designed with different level numbers of phase gradient under the illumination of a single wavelength (λ = 500 nm). Peak conversion efficiency as a function of (c) incident wavelength with the level number of phase gradient fixed at 8 and (d) level number at the fixed incident wavelength of λ = 500 nm obtained from panels a and b, respectively. All of the incident waves are polarized along the horizontal x-axis.

referred to as geometric phase) method to realize the optimal control of the CP phase. Unlike the commonly used phase modulation methods in metasurfaces that rely on multi-resonances determined by metal patterns of varying sizes arranged along a particular orientation,[25] the P−B phase method achieves phase modulation through space-variant optical axis orientations of the plasmonic structures of equal dimensions.[26] Because of the space-invariant structural dimensions, such a technique offers the advantage of decoupling the phase modulation from the amplitude modulation for the scattered light at a fixed incident wavelength. In addition, the P−B phase method applied to Al plasmonic metasurfaces works independently at each wavelength over the wide visible and UV range, making it feasible for broadband operation. Here we demonstrated a single MPG device with Al plasmonic structures that produces four LPs (horizontal, vertical, +45°, and −45°) and two CPs (left-hand, LCP and right-hand, RCP) from a single linearly polarized source. Owing to the anomalous reflectance of the P−B phase method implemented with phase-modulating supercells of different lengths, all six light beams of different polarizations split into six directions, making them convenient to be used as subsequent light sources and easy to detect and analyze as they emerge background free at angles different from either the incident light source or normal reflection of the metasurface (Figure 1a). The spatial offset between the nearby supercells of equal length is used to induce the needed phase delay between LCP and RCP that are reflected to the same anomalous angle so that their superposition can produce light wave of any desired polarization.

Design of the Metasurface Polarization Generator. The basic building blocks of MPG are Al nanoantennas of equal size. When they are all arranged parallel along a fixed direction, an incident wave of LCP can be converted to that of RCP and vice versa. Figure 1b shows the optical characteristic of Al nanoantennas of equal dimensions of 170 nm × 50 nm × 50 nm patterned with the period of 230 nm × 230 nm along the same orientation on a SiO_2 layer over a 150 nm thick Al mirror deposited on a Si substrate. The SiO_2-layer thickness is optimized for high conversion efficiency while minimizing co-polarization reflectance and absorption[27] of the Al nanoantenna/SiO_2/Al film structure (see Supporting Information (SI), part 1). To achieve polarization conversion for circularly polarized light in a wide range of wavelength, the Al nanoantenna needs to exhibit two fundamental resonances that are separated far apart in wavelength, one along its long axis and the other short axis, acting as a half-wave plate[28] (see SI, part 2). According to our simulation, the conversion efficiency for either LCP-to-RCP or RCP-to-LCP remains above ∼50% over the visible region of 400−700 nm when the SiO_2-layer thickness is chosen to be 50 nm. For longer wavelengths beyond 700 nm, interband transitions in Al begin to induce significant loss[23,29,30] and cause conversion efficiency to drop. To extend its operation into the infrared, other metals such as Ag or Au can be considered with Ag holding some advantage over Au for being of lower loss but suffering from oxidization which can limit its functionality.

We then employed the P−B phase method by rotating the orientations of nanoantennas gradually with a constant step size of θ from 0 to π to create a supercell as shown in Figure 1c. Each orientation angle change of θ will result in a 2θ phase

DOI: 10.1021/acs.nanolett.6b04446
Nano Lett. 2017, 17, 445−452

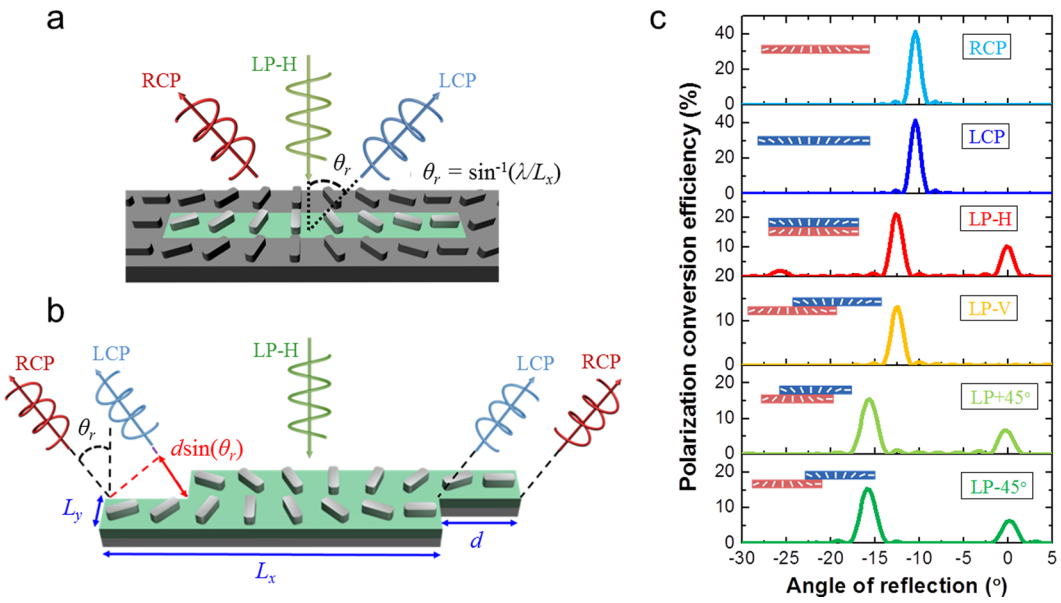

Figure 3. Polarization generation with superposition of CPs. Schematics for (a) circular polarization generation through intrinsic property of P−B phase-based metasurfaces and (b) linear polarization generation through superposition of CPs under an *x*-polarized (LP-H) light illumination. (c) Simulated conversion efficiency for each polarization at the incident wavelength of 500 nm. All insets present the schematic of corresponding supercell design. The lengths of supercells L_x for RCP and LCP, LP-H and LP-V, and LP+45° and LP−45° are 2.76 μm, 2.3 μm, and 1.84 μm, respectively.

change for the impinging CP light, resulting in 0-to-2π phase modulation. Because of the equal dimensions of these nanoantennas, the conversion efficiency mostly determined by the amplitude modulation remains unchanged with respect to the various locations in the supercell. As a result, metasurfaces made of these supercells have the ability to modulate phase without significant relative amplitude modification at different positions, which forms the underlining design principle of our MPG device. To demonstrate this, we have simulated the phase modulation and conversion efficiency—a measure of amplitude modulation for eight periodical arrays, each made of Al nanoantennas of equal dimensions arranged in a particular angle θ, as illustrated in Figure 1c. Indeed, 2π-phase modulation can be achieved, and the conversion efficiency for each set of antennas at a fixed orientation is reasonably flat at about 73% at the wavelength of 500 nm. A subsequent construction of a supercell with 8 Al nanoantennas each orientated with the augmenting angle step of $\pi/8$ (the number of Al nanoantennas in a supercell is also referred to as number of levels for the phase modulation) should produce the needed 2π-phase modulation without the amplitude modulation. A MPG device can be designed and fabricated by arranging such supercells in various patterns (Figure 1a) at different locations of the metasurface to achieve the necessary phase gradients for the desired polarization light beams to be scattered into predetermined anomalous reflection angles.

According to the generalized Snell's law,[31] the angle of anomalous reflection θ_r from a MPG can be determined by the incident wavelength λ in free space and supercell length L_x, as $\theta_r = \sin^{-1}(\lambda/L_x)$ under a normal illumination. For example, when the length of supercell is fixed (i.e., the number of Al nanoantennas in a supercell is fixed since each nanoantenna occupies a fixed unit area of 230 nm × 230 nm in our design), the angle of anomalous reflection becomes larger when the incident wavelength is longer, as shown by simulation in Figure 2a. The result also indicates the P−B phase-based MPG made of Al nanoantenna supercells works well across the visible spectral range. The simulated conversion efficiency has been plotted as a function of wavelength in Figure 2c and can be found to reach maximum at λ = 500 nm, consistent with the prediction from the simulation result in Figure 1b. The number of levels (or the number of Al nanoantennas in a supercell) employed in the phase gradient also plays a role in the angle of anomalous reflection because higher level numbers require a greater supercell length to implement since each Al nanoantenna occupies a fixed unit area as shown in Figure 2b. We have found through simulation that the maximum CP conversion efficiency increases with the level number of phase gradient as shown in Figure 2d. It is not difficult to see that the higher level number offers a smoother phase gradient across the metasurface, resulting in higher conversion efficiency.[32] But the conversion efficiency tends to reach a plateau when the level number surpasses 8. We therefore choose to keep the minimum level number of phase gradient at 8 as we design the MPG.

We now discuss the design principle of the MPG using the above simulation results obtained from the Al metasurface. Considering that the MPG reflects a LCP light beam at normal incidence to a RCP light with its phase gradient at an anomalous angle $+\theta_r$, then a RCP at normal incidence will result in a LCP reflection at $-\theta_r$. By reversing the order of the supercells arranged on the metasurface, we arrive at inverse optical response from the original polarization.[26] As a result, a LP light which can be viewed as a combination of LCP and RCP, upon impinging upon the metasurface, will create two CP reflection beams with opposite handedness propagating in two different directions, $\pm\theta_r$, simultaneously, as shown in Figure 3a. Once LCP and RCP are produced, we can use them to generate LP states by simply superpositioning the orthogonal LCP and RCP through combining two supercells with opposite nanoantenna orientations. The MPG consists of two supercells with

DOI: 10.1021/acs.nanolett.6b04446
Nano Lett. 2017, 17, 445−452

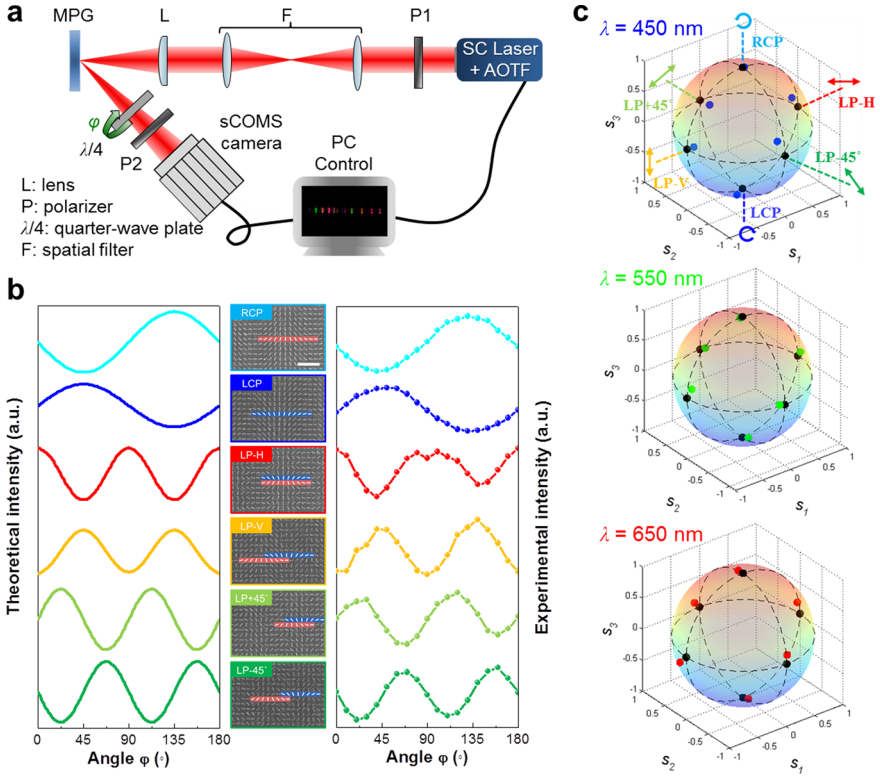

Figure 4. Experimental verification of generated polarizations. (a) Measurement setup for the MPG characterization. (b) Theoretical (left column) and experimental (right column) diagram of scattering intensity as a function of rotating angle of the quarter-wave plate. Here, the LP-H incident wavelength λ = 600 nm. Middle column: corresponding SEM images with a 1 μm scale bar. Six lines display the results for six polarizations. (c) Poincaré sphere experimental results (red/green/blue dots) compared with theoretical predictions (black dots) for different incident wavelengths.

a position offset d, providing a phase difference between the two CPs needed to produce LP scattered wave along a particular direction[33] (see Figure 3b). Basically, the RCP ($|R\rangle$) and LCP ($|L\rangle$) waves can be respectively described in terms of Jones vectors as

$$|R\rangle = \frac{1}{\sqrt{2}}\begin{bmatrix}1\\-i\end{bmatrix}$$

$$|L\rangle = \frac{1}{\sqrt{2}}\begin{bmatrix}1\\i\end{bmatrix} \quad (1)$$

The position offset d between two supercells is implemented to yield a phase delay $\alpha = k_0 d \sin(\theta_r) = 2\pi d/L_x$ between the two scattered LCP and RCP. Here, $k_0 = 2\pi/\lambda$ is the wavenumber in free space. The superposition of these two CP waves can then be given as

$$|n\rangle = |R\rangle + e^{i\alpha(d,L_x)}|L\rangle \quad (2)$$

where $|n\rangle$ represents a LP wave when the position offset d is chosen properly with a fixed length of supercell L_x. For demonstration purposes, we have put together two supercells with different position offsets to generate six kinds of polarizations all from a single MPG device, including LCP, RCP, LP along horizontal (LP-H) corresponding to x polarization, LP along vertical (LP-V) corresponding to y polarization, LP along +45° (LP+45°), and RP along −45° (LP−45°). Since the angle of anomalous reflection is related to the length of supercell which is determined by the level number of phase gradient at a fixed wavelength, we can separate the different polarization beams into different reflection angles by adopting three phase-gradient level numbers: 8 for LP+45° and LP−45°, 10 for LP-H and LP-V, and 12 for LCP and RCP, making these different polarization beams easily separated from one another as well as from incident and normal reflection waves. Figure 3c shows the numerical simulation results for the conversion efficiency of the scattering light of different polarizations for three structural configurations. The anomalous reflection angle of scattered light with designed polarizing state agrees almost exactly with the generalized Snell's law. The six polarizing states can be observed by detecting their electric field components generated by these three structural configurations, as shown in Figure 3c. It is worth mentioning that the level number of phase gradient can be chosen at will, and one can obtain a given polarization state at any desired observation angle.

Experimental Characterization of Metasurface Polarization Generator. The Stokes vector described below can be conveniently used to evaluate any polarization states:

$$S = \begin{bmatrix}S_0\\S_1\\S_2\\S_3\end{bmatrix} = \begin{bmatrix}|E|^2\\|E_{LHP}|^2 - |E_{LVP}|^2\\|E_{L+45P}|^2 - |E_{L-45P}|^2\\|E_{RCP}|^2 - |E_{LCP}|^2\end{bmatrix} \quad (3)$$

where the Stokes parameters S_i (i = 0, 1, 2, and 3) are a set of values related to the amplitudes of polarizing states. Figure 4a shows the optical setup to measure the Stokes parameters and characterize the generated polarizing states of the fabricated MPG under a LP-H wave illumination at normal incidence. A

DOI: 10.1021/acs.nanolett.6b04446
Nano Lett. 2017, 17, 445−452

supercontinuum laser combined with an acousto-optic tunable filter was employed to generate a series of discrete laser peaks at a desired incident wavelength. Polarizer (P1) is used to generate a LP-H beam from the incident laser source. Upon impinging on the MPG, the scattered light was projected onto the focal plane of the lens (L). Light diffracted by the MPG then goes through a broadband quarter-wave plate ($\lambda/4$) and another polarizer (P2) and is then collected by a sCMOS camera. The distance between the MPG and sCMOS camera is optimized for detecting simultaneously all six scattered light spots with different polarizations (see SI, part 3). We subsequently obtain a plot of signal intensity as a function of reflection angle of fast axis φ of quarter-wave plate. The intensity variation can be calculated by the Mueller matrix:[34]

$$I(\varphi) = \frac{1}{2}[A - B\sin(2\varphi) + C\cos(4\varphi) + D\sin(4\varphi)] \tag{4}$$

where

$$A = \frac{1}{\pi}\int_0^{2\pi} I(\varphi)\,\mathrm{d}\varphi$$

$$B = \frac{1}{\pi}\int_0^{2\pi} I(\varphi)\sin(2\varphi)\,\mathrm{d}\varphi$$

$$C = \frac{1}{\pi}\int_0^{2\pi} I(\varphi)\cos(4\varphi)\,\mathrm{d}\varphi$$

$$D = \frac{1}{\pi}\int_0^{2\pi} I(\varphi)\sin(4\varphi)\,\mathrm{d}\varphi \tag{5}$$

These parameters are related to Stokes parameters as $S_0 = A - C$, $S_1 = 2C$, $S_2 = 2D$, $S_3 = B$ (see SI, part 4), and therefore all Stokes parameters of scattered light from the designed MPG can be obtained via the scattered intensity with respect to φ. We have fabricated a MPG device consisting of six areas, each made of one type of supercells responsible for generating a light beam of a particular polarizing state into a predetermined scattering angle. The six different areas fabricated using electron beam lithography on a single metasurface chip are shown in the center column of Figure 4b along with their theoretical and experimental results for the LP-H incident wave at λ = 600 nm where lines of different color represent different polarizations and correspond to their SEM images of the same labeled color. The theoretical and measured results show a good agreement. The slight difference can be attributed to the imperfect shapes of the Al nanoantennas, surface oxidization of Al nanoantennas, and alignment issue in the optical measurement as well as nonideal optical components (especially the quarter-wave plate). These results can be plotted on the Poincaré sphere for evaluation of generated polarizing states.

Implementing the Stokes parameters as the sphere's coordinates, the Poincaré sphere offers a prominent three-dimensional space geometric representation of polarization. Any polarizing state can be uniquely described as a point on or within a unit sphere. It is a convenient presentation that makes polarization transformation clear to view. Figure 4c shows the comparison of experimental results (color dots) and theoretical predictions (black dots) at three different wavelengths, red (650 nm), green (550 nm), and blue (450 nm). Again, the measured results show a good agreement with the theoretical prediction. More experimental results are presented in the SI, validating that the proposed MPG is indeed capable of operating in the broad visible spectrum.

Discussion. The performance of the MPG is further analyzed by measuring the extinction ratio of a given generated polarization. This is done by examining the ratio of optical power of the desired polarization to that of its orthogonal counterpart. The experimental results indicate that all generated polarizing states delivered high extinction ratios over the wide range of visible spectrum, as shown in Figure 5.

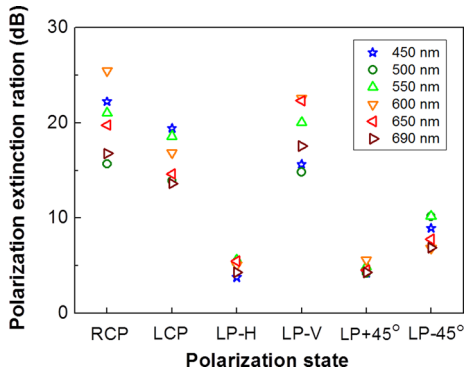

Figure 5. Polarization extinction ratio. Measured polarization extinction ratio of the six generated polarizing states over a wide range of visible light.

These extinction ratios are significantly higher than those of previously reported from either metamaterials or metasurfaces, and the purity of generated polarization is on par with commercial products. In addition to the high polarization extinction ratio, the anomalous reflection beam of a given polarizing state allowed for its background-free detection by conveniently avoiding the experimental setup complication arising from the incident and normal reflective signals during the measurement. We could have easily designed the MPG to produce elliptically polarized wave in addition to the LP and CP waves by simply tuning the position offset d. Such MPG can also work as a polarization-dependent beam splitter to decompose any incident light into two orthogonal polarizations and separate them into different angles.

Conclusions. We have demonstrated a MPG capable of generating multiple polarization waves with a high polarization extinction ratio in a reflective scheme. Using Al nanoantennas of equal dimensions as the basic building blocks and achieving phase modulation through tuning of their optical axis orientations, we have designed and fabricated the MPG consisting of six areas, each with a patterned array of supercells made of Al nanoantennas arranged with an incremental step of orientating angle to realize the 2π-phase modulation without significant relative amplitude modification at different locations of the metasurface. We have implemented in a supercell with the level number of phase gradient no less than 8 to yield six different polarization beams all with high polarization conversion efficiency and demonstrated that the Al plasmonic MPG can indeed operate in the wide visible spectrum. The reflective MPG device fabricated on top of a SiO_2/Al/Si ground plate has produced a much higher conversion efficiency than that of transmission type previously reported by other groups. To further increase the conversion efficiency, it is desirable to replace any metal on the MPG with patterned low-loss dielectric features made of materials such as TiO_2, GaN, and so forth, as the active components that interact with incident

DOI: 10.1021/acs.nanolett.6b04446
Nano Lett. 2017, 17, 445−452

and scattered light for polarization generation. The purity of polarization is the highest among all reported with either metamaterials or metasurfaces and on par with commercial products. The low cost and ease of adaptability to various platforms make Al plasmonic MPGs particularly promising with low economic threshold for mass production and thus can be made widely available for a broad range of applications. In comparison with commercial polarization generators/modulators that are available in the market, our MPG device is optical thin, easy to fabricate, and compatible with flat optics. With the validation of generating multiple waves of different polarizations from a single metasurface, we demonstrate that MPG made of Al is an effective and versatile optical component that can be integrated in photonic circuits and potentially expands the reach of nanotechnology.

Methods. *Fabrication of MPG.* All samples are prepared by standard electron beam lithography and lift-off process. A 150-nm-thick aluminum mirror and 50-nm-thick SiO_2 were first deposited by magnetron sputtering machine (Shibaura Mechatronics Corp.) on a silicon substrate. The 495 K PMMA (poly(methyl methacrylate)) photoresist was then deposited by spin coating and baked at 180 °C for 3 min. Before the e-beam exposure, a conductive polymer layer Espacer, which can be directly removed by rinsing with deionized water is spin-coated over the PMMA layer to eliminate the charging issue. After electron beam exposure with 30 pA current, the sample was developed in a solution of isopropyl alcohol (IPA) and methyl isobutyl ketone (MIBK) of IPA:MIBK = 3:1 for 60 s, followed by removing Espacer with deionized water. The sample was subsequently rinsed with IPA and blow-dried with nitrogen gun. Aluminum with the desired thickness was then deposited via e-beam evaporator. The aluminum nanoantennas were consequently defined on the substrate after the lift-off process.

Simulation. All simulation results were performed with the commercial software CST Microwave Studio. For the case of single cell design, a unit cell boundary condition is employed for the simulation of reflection and phase shift in an array structure. The refractive index of SiO_2 is obtained from ref 35. The permittivity of aluminum in the visible regime is described by the Drude model.

■ ASSOCIATED CONTENT

Supporting Information

The Supporting Information is available free of charge on the ACS Publications website at DOI: 10.1021/acs.nanolett.6b04446.

Detailed information on optical responses for aluminum-nanoantenna/SiO_2/aluminum-mirror structure, fundamental resonances and half-wave plate behavior of Al nanoantenna, camera images of generated polarizing states, description of Stokes parameters via Mueller matrix, and additional experimental results (PDF)

■ AUTHOR INFORMATION

Corresponding Author

*E-mail: dptsai@phys.ntu.edu.tw.

ORCID

Din Ping Tsai: 0000-0002-0883-9906

Author Contributions

P.C.W. and W.Y.T. contributed equally to this work.

Notes

The authors declare no competing financial interest.

■ ACKNOWLEDGMENTS

The authors acknowledge financial support from Ministry of Science and Technology, Taiwan (Grant No. MOST-105-2745-M-002-002-ASP) and Academia Sinica (Grant No. AS-103-TP-A06). They are also grateful to National Center for Theoretical Sciences, NEMS Research Center of National Taiwan University, National Center for High-Performance Computing, Taiwan, and Research Center for Applied Sciences, Academia Sinica, Taiwan for their supports. G. Sun acknowledges support from AFOSR (FA9550-14-1-0196) and AOARD (FA2386-16-1-4069).

■ REFERENCES

(1) Bahadur, B. *Mol. Cryst. Liq. Cryst.* **1984**, *109*, 3−93.
(2) Calabretta, N.; Liu, Y.; Huijskens, F. M.; Hill, M. T.; de Waardt, H.; Khoe, G. D.; Dorren, H. J. S. *J. Lightwave Technol.* **2004**, *22*, 372−381.
(3) Young, L.; Robinson, L.; Hacking, C. *IRE Trans. Antennas Propag.* **1973**, *21*, 376−378.
(4) Mühlschlegel, P.; Eisler, H. J.; Martin, O. J. F.; Hecht, B.; Pohl, D. W. *Science* **2005**, *308*, 1607−1609.
(5) Hariharan, P. C.; Pople, J. A. *Theoretica chimica acta* **1973**, *28*, 213−222.
(6) Walther, P.; Resch, K. J.; Rudolph, T.; Schenck, E.; Weinfurter, H.; Vedral, V.; Aspelmeyer, M.; Zeilinger, A. *Nature* **2005**, *434*, 169−176.
(7) Dickson, R. M.; Norris, D. J.; Tzeng, Y.-L.; Moerner, W. E. *Science* **1996**, *274*, 966−968.
(8) Smith, D. R.; Pendry, J. B.; Wiltshire, M. C. K. *Science* **2004**, *305*, 788−792.
(9) Gharghi, M.; Gladden, C.; Zentgraf, T.; Liu, Y.; Yin, X.; Valentine, J.; Zhang, X. *Nano Lett.* **2011**, *11*, 2825−2828.
(10) Wu, P. C.; Chen, W. T.; Yang, K.-Y.; Hsiao, C. T.; Sun, G.; Liu, A. Q.; Zheludev, N.; Tsai, D. P. *Nanophotonics* **2012**, *1*, 131−138.
(11) Huang, Y.-W.; Chen, W. T.; Wu, P. C.; Fedotov, V. A.; Zheludev, N. I.; Tsai, D. P. *Sci. Rep.* **2013**, *3*, 1237.
(12) Gansel, J. K.; Thiel, M.; Rill, M. S.; Decker, M.; Bade, K.; Saile, V.; von Freymann, G.; Linden, S.; Wegener, M. *Science* **2009**, *325*, 1513−1515.
(13) Zhao, Y.; Belkin, M. A.; Alù, A. *Nat. Commun.* **2012**, *3*, 870.
(14) Minovich, A. E.; Miroshnichenko, A. E.; Bykov, A. Y.; Murzina, T. V.; Neshev, D. N.; Kivshar, Y. S. *Laser Photon. Rev.* **2015**, *9*, 195−213.
(15) Ding, F.; Wang, Z.; He, S.; Shalaev, V. M.; Kildishev, A. V. *ACS Nano* **2015**, *9*, 4111−4119.
(16) Zhao, Y.; Alù, A. *Nano Lett.* **2013**, *13*, 1086−1091.
(17) Aieta, F.; Genevet, P.; Kats, M. A.; Yu, N.; Blanchard, R.; Gaburro, Z.; Capasso, F. *Nano Lett.* **2012**, *12*, 4932−4936.
(18) Chen, X.; Huang, L.; Mühlenbernd, H.; Li, G.; Bai, B.; Tan, Q.; Jin, G.; Qiu, C.-W.; Zhang, S.; Zentgraf, T. *Nat. Commun.* **2012**, *3*, 1198.
(19) James, T. D.; Mulvaney, P.; Roberts, A. *Nano Lett.* **2016**, *16*, 3817−3823.
(20) Olson, J.; Manjavacas, A.; Liu, L.; Chang, W.-S.; Foerster, B.; King, N. S.; Knight, M. W.; Nordlander, P.; Halas, N. J.; Link, S. *Proc. Natl. Acad. Sci. U. S. A.* **2014**, *111*, 14348−14353.
(21) Yokogawa, S.; Burgos, S. P.; Atwater, H. A. *Nano Lett.* **2012**, *12*, 4349−4354.
(22) Miyata, M.; Hatada, H.; Takahara, J. *Nano Lett.* **2016**, *16*, 3166−3172.
(23) Huang, Y.-W.; Chen, W. T.; Tsai, W.-Y.; Wu, P. C.; Wang, C.-M.; Sun, G.; Tsai, D. P. *Nano Lett.* **2015**, *15*, 3122−3127.

DOI: 10.1021/acs.nanolett.6b04446
Nano Lett. 2017, 17, 445−452

(24) Ding, X.; Monticone, F.; Zhang, K.; Zhang, L.; Gao, D.; Burokur, S. N.; de Lustrac, A.; Wu, Q.; Qiu, C.-W.; Alù, A. *Adv. Mater.* **2015**, *27*, 1195−1200.
(25) Yu, N.; Capasso, F. *Nat. Mater.* **2014**, *13*, 139−150.
(26) Huang, L.; Chen, X.; Mühlenbernd, H.; Li, G.; Bai, B.; Tan, Q.; Jin, G.; Zentgraf, T.; Zhang, S. *Nano Lett.* **2012**, *12*, 5750−5755.
(27) Landy, N. I.; Sajuyigbe, S.; Mock, J. J.; Smith, D. R.; Padilla, W. J. *Phys. Rev. Lett.* **2008**, *100*, 207402.
(28) Khorasaninejad, M.; Crozier, K. B. *Nat. Commun.* **2014**, *5*, 5386.
(29) Knight, M. W.; King, N. S.; Liu, L.; Everitt, H. O.; Nordlander, P.; Halas, N. J. *ACS Nano* **2014**, *8*, 834−840.
(30) Sobhani, A.; Manjavacas, A.; Cao, Y.; McClain, M. J.; García de Abajo, F. J.; Nordlander, P.; Halas, N. J. *Nano Lett.* **2015**, *15*, 6946−6951.
(31) Yu, N.; Genevet, P.; Kats, M. A.; Aieta, F.; Tetienne, J.-P.; Capasso, F.; Gaburro, Z. *Science* **2011**, *334*, 333−337.
(32) Zheng, G.; Mühlenbernd, H.; Kenney, M.; Li, G.; Zentgraf, T.; Zhang, S. *Nat. Nanotechnol.* **2015**, *10*, 308−312.
(33) Yu, N.; Aieta, F.; Genevet, P.; Kats, M. A.; Gaburro, Z.; Capasso, F. *Nano Lett.* **2012**, *12*, 6328−6333.
(34) Goldstein, D. *Polarized Light*, 3rd ed.; CRC Press, 2016.
(35) Ghosh, G. *Opt. Commun.* **1999**, *163*, 95−102.

DOI: 10.1021/acs.nanolett.6b04446
Nano Lett. 2017, 17, 445−452